Materials Research Express

PAPER

Understanding temperature and magnetic-field actuated magnetization polarity reversal in the Prussian blue analogue $Cu_{0.73}Mn_{0.77}[Fe(CN)_6].zH_2O$, using XMCD

RECEIVED
27 August 2015

REVISED
17 November 2015

ACCEPTED FOR PUBLICATION
8 February 2016

PUBLISHED
24 February 2016

Debdutta Lahiri[1], **Yongseong Choi**[2], **S M Yusuf**[3], **Amit Kumar**[3], **Nitya Ramanan**[1], **Soma Chattopadhyay**[2,4], **Daniel Haskel**[2] **and Surinder M Sharma**[1]

[1] High Pressure & Synchrotron Radiation Physics Division, Bhabha Atomic Research Centre, Mumbai-400085, India
[2] Advanced Photon Source, Argonne National Laboratory, Argonne, IL 60439, USA
[3] Solid State Physics Division, Bhabha Atomic Research Centre, Mumbai-400085, India
[4] Physical Sciences Department, Elgin Community College, 1700 Spartan Drive, Elgin, IL 60123, USA

E-mail: dlahiri@barc.gov.in **and** smyusuf@barc.gov.in

Keywords: XMCD, negative magnetization, magnetic switch, Prussian blue analog, molecular magnet

Supplementary material for this article is available online

Abstract

We have investigated the microscopic origin of temperature and magnetic-field actuated magnetization reversal in $Cu_{0.73}Mn_{0.77}[Fe(CN)_6].zH_2O$, using XMCD. Our results show a fair deviation from the mean-field-theory in the form of different ordering temperatures of Fe and Mn sublattices. A preferential sign reversal of Mn spin under magnetic field and different spin cant angles for the two sublattices have also been observed. An antiferromagnetic coupling between the Fe and Mn sublattices along with different ordering temperatures (sublattice decoupling) for these sublattices explain the temperature-dependent magnetization reversal. Whereas, Mn spin reversal alone (under external magnetic field) is responsible for the observed field-dependent magnetization reversal. The dissimilar magnetic behavior of Fe and Mn sublattices in this cubic 3d-orbital system has been understood by invoking disparity and competition among inter-sublattice magnetic control parameters, viz. magnetic Zeeman energy, exchange coupling constant and magnetic anisotropy constant. Our results have significant design implications for future magnetic switches, by optimizing the competition among these magnetic control parameters.

1. Introduction

The phenomenon of magnetization reversal or negative magnetization across a compensation temperature with zero net magnetization has drawn a lot of attention in recent years due to its fundamental and technological implications in magnetic memory, magneto-caloric, spin resolving devices, etc [1 and references therein]. The study of magnetization of individual sublattices across the compensation temperature using a microscopic technique is very much essential for understanding of the phenomenon. Magnetization reversal, observed in several classes of materials [1 and references therein], has been explained within the framework of mean-field-theory (MFT) [2], proposed by Néel assuming a common magnetic ordering temperature for all the magnetic sublattices [3, 4].

Exceptional cases, such as multiple ordering temperatures or sub-lattice decoupling, have been reported for systems where the basic conditions of MFT are violated e.g. heterogeneous systems (e.g. phase segregation, non-equivalent defect sites, size effect [5, 6]) or rare earth compounds with highly localized orbital [7–12]. Though these reports [5–12] could capture the individual sub-lattice ordering, they fail to bring out the rich intricate physics involved in magnetization reversal process e.g. importance of non-exchange interaction, such as magnetic-anisotropy energy (MAE), and a competition among MAE, exchange energy (E_{exch}), and Zeeman energy (ZE) [1, 13, 14].

In this work, we address the issue of non-MFT behavior of magnetic sublattices in Prussian blue analogue (PBA) compound, $Cu_{0.73}Mn_{0.77}[Fe(CN)_6].zH_2O$ [15–17], for which some of us had reported the novel magnetization reversal phenomenon as depicted in figure S1 (supplementary information file). We bring out the importance of MAE, E_{exch} and ZE [1, 13, 14] to explain the magnetization reversal phenomenon as a function of temperature (T) and magnetic field (H). At low (200 Oe) field condition, multiple ($\times 2$) magnetic transitions occur in the PBA system at $(T_{CR1}, T_{CR2}) = (8.8\ \text{K},\ 17.9\ \text{K})$ (figure S1). Out of these, T_{CR1} (=8.8 K) indicates the onset of magnetization reversal (from positive to negative) with decreasing temperature. However, magnetization under high (1 kOe) applied field remains positive down to the lowest temperature (figure S1). A low field actuated magnetization (μ_{net}) reversal (or magnetization flip-flop transition) (figure S1), from negative to positive, was also demonstrated in this system below 8.8 K. The magnetization crossover, being reversible and reproducible, establishes bi-stable (flip-flop) magnetization states, important for applications in magnetic memory [18] and self-driven magnetic refrigerator [19–21]. We take the same PBA system as a case study to derive magnetization of individual sublattices across the magnetization compensation temperature T_{CR1}, and also under the effect of an external magnetic field. We have used x-ray magnetic circular dichroism (XMCD) technique. For the present compound, temperature as well as magnetic field dependent magnetization reversal occurs below the Mn sublattice ordering temperature, which is 13.5 K for the Mn-based end compound $Mn_{1.5}Fe(CN)_6$ [15]. This raises important questions: (i) Whether Mn sublattice orders separately from Fe/Cu sublattices in the present three-sublattice system, (ii) What is the role of Mn sublattice ordering for stabilization of negative magnetization? (iii) Whether field-induced magnetization sign reversal entails spin flip of Mn? (iv) What are the basic interactions involved in the field induced magnetization reversal? and (v) How do these interactions lead to the decoupling (non-MFT behavior) of Mn sublattice ordering?

For the present PBA, the scope of the earlier neutron diffraction study, a microscopic tool to understand magnetic sublattice ordering, was limited and could be performed only at $(T = 1.7\ \text{K},\ H = 0)$ [15]. A meaningful neutron diffraction study at higher temperatures ($T > 1.7$ K) was not possible due to the presence of a large diffuse scattering arising from the structural defects/water molecules. We have now employed XMCD technique to derive $\mu(H,\ T)_{Fe,Mn}$ across the compensation temperature for the present PBA compound. XMCD is based on spin-resolved difference in absorption cross-section, and measures the magnetic moment via spin polarization of the empty states of an element [22]. The required reference direction for spin-resolved *an*alysis is defined by the helicity of circularly polarized synchrotron photons. By measuring XMCD at the edges of component elements, sub-lattice resolved magnetic moments can be derived [7–12, 22]. Ideally, $L_{2,3}$ edge-XMCD ($2p \rightarrow 3d$) should be employed to probe d-states. However, $L_{2,3}$ edge-experiments require a vacuum environment. Since moisture content is important for our sample [23], it could not be placed in vacuum to prevent the loss of H_2O molecules. Therefore, K-edge XMCD ($1s \rightarrow 4p$) is employed, in which the XMCD signal is proportional to spin-polarized 4p-projected density of states. This determines 3d-moment *indirectly* via 4p–3d exchange interaction [24]. Although this indirect method is unable to determine the absolute values of the magnetic moments, it adequately provides a comparative insight of the magnetic sublattices (ordering temperature, spin cant angle, etc) [25, 26].

Using the XMCD results, we demonstrate: (i) separate ordering temperatures of (Fe, Mn) sublattices viz. $(T_{Mn},\ T_{Fe}) \approx (8.8\ \text{K},\ 18.9\ \text{K})$; (ii) field-induced preferential spin reversal of Mn sublattice; and (iii) canted spin configuration of Fe sublattice. All of these reflect dissimilarity between (Fe, Mn) sublattices. We establish that temperature-and field-induced magnetization sign reversal processes are, respectively, associated with spin ordering and spin reversal of Mn sublattice. By considering the inter-sublattice disparity of magnetic parameters (exchange coupling constant, magnetic moments i.e. ZE, and anisotropy constant) and field / temperature-dependent hierarchy of the interaction forces, we are able to account for the magnetic dissimilarity of (Fe, Mn) sublattices. This is the first 3d-orbital system where *intrinsic* sublattice decoupling, arising out of competition among the above-mentioned magnetic forces, is reported. This work should inspire design of future magnetic switches by systematically optimizing these magnetic control parameters.

2. Experimental methods

Sample synthesis and initial magnetic characterizations are detailed in [15–17]. Since the sample is sensitive to moisture and light, it was handled with special precaution. As-prepared sample was covered in black paper before being transported to the advanced photon source (APS), USA. The powdered sample (of grain size $\sim 10\ \mu$m) was pasted on a tape inside a glove box. During this procedure, the bright lights in the room were switched off and the surrounding areas of the sample were covered by a black paper to minimize the amount of direct light hitting the sample. After sample preparation was complete, the black paper was removed and the tape sample was transferred out of glove box into a displex cryostat sample holder for low-temperature XMCD experiments. In order to preserve the H_2O content, the sample could *not* be placed directly into the vacuum

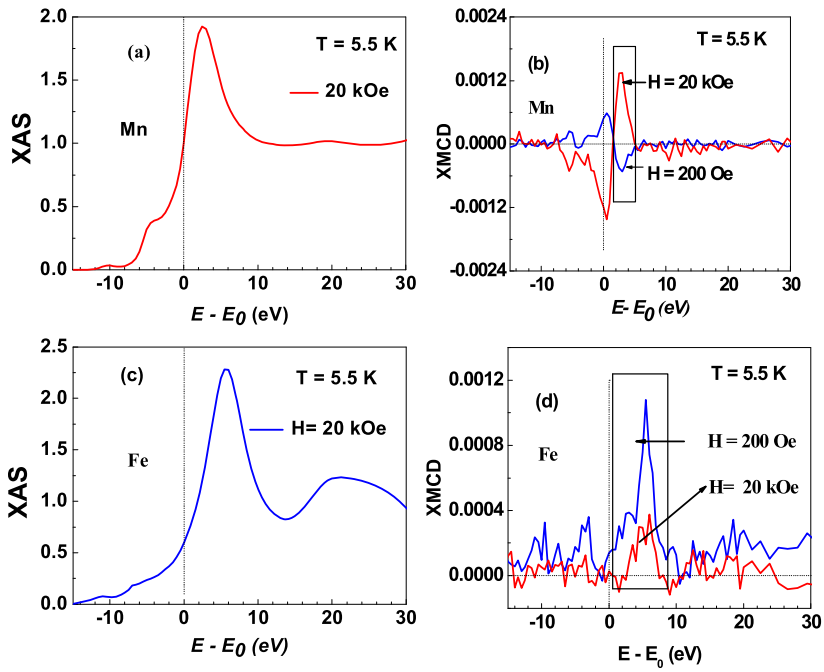

Figure 1. XANES at $T = 5.5$ K at (a) Mn and (c) Fe K-edges. XMCD at $T = 5.5$ K at (b) Mn and (d) Fe K-edges. There is unambiguous sign reversal between the two field conditions, for Mn sub-lattice in (a).

environment of the cryostat. An extra He-filled shroud, with Kapton-sealed windows, was inserted between the inner sample holder and displex. Both the inner sample holder and extra He-filled shroud were made of non-magnetic Al 6061 alloy [27], and assembled inside the He-filled glove box.

X-ray absorption spectroscopy (XAS) or x-ray absorption near edge structure (XANES) on field-cooled samples were measured at 4-ID-D beamline (Undulator A) of APS [28]. Si(111) monochromator was used to filter out Mn, Fe and Cu K-edges (6.3–9.5 keV) and the energy was calibrated by measuring XAFS on foils at the respective edges. Circularly polarized x-rays were generated with 180 μm thick diamond (111) phase plate. XAS for different helicities (I^+, I^-) were measured in transmission-mode using photo-diodes. At each edge, XMCD signal was obtained by switching the helicity (+, −) [29] (with respect to applied magnetic field) and measuring the related modulation in XAS signal $\left(\Delta I = \frac{I^+ - I^-}{2}\right)$ with a lock-in-amplifier; the polarization rates are $P_c = 0.91, P_c = 0.95, P_c = 0.96$ at Cu, Fe and Mn K-edges, respectively. The asymmetry ratio R (XMCD signal) was obtained by normalizing ΔI relative to the average XAS signal $\left(I = \frac{I^+ + I^-}{2}\right)$ i.e. $R = \frac{\Delta I}{I}$. The offsets in lock-in-amplifier output were eliminated by measuring R for two opposite field directions ($H+$ and $H-$), and the final XMCD signal was determined to be $(R^{H+} - R^{H-})$[29]. These XMCD measurements were performed, covering the magnetic field and temperature range of the observed magnetization polarity reversal viz. $H = 200$ Oe (non-flip), and $H = 20$ kOe (flip) over 5–30 K. XAS spectra ($T = 5.5$ K, $H = 20$ kOe) at Mn and Fe K-edges are shown in figures 1(a) and (c), respectively. XMCD spectra, at $T = 5.5$ K for both field conditions are shown in figures 1(b) and (d).

Cu K-edge XMCD signal was very low for an unambiguous analysis, and could be due to small magnetic moment of Cu. (Cu K-edge XAS and XMCD spectra are shown in figures S2(a) and (b) respectively.) For subsequent analysis of the XMCD data, a strong ferromagnetic coupling between Fe and Cu moments is assumed and an ordered magnetic moment of $\sim 1\ \mu_B$ for Cu is considered, as reported in the low temperature neutron diffraction study [15].

We note that the interpretation and quantification of the K-edge XMCD is still controversial. In our analysis, we assume (like in past studies [26]) that for each field and temperature condition, Mn and Fe 4p moments (μ_{Mn}, μ_{Fe}) (in arbitrary units) are proportional to the integrated area of their respective XMCD peaks. The area was calculated to be the sum of $(R^{H+} - R^{H-})$ over all the data points covered in the peak range 1.5–5 eV and 0–10 eV (*with respect to* E_0) for Mn and Fe K-edges, respectively. (Details of area and error calculation are provided in supplementary material.) As mentioned earlier in section 1, K-edge XMCD-derived 4p moments (μ_{Mn}, μ_{Fe}) reflect 3d moment values. Experimentally testing the proportionality between 3d spin/orbital and 4p orbital moments, for different temperature and field conditions, is beyond the scope of the current paper. The important (and advantageous) point is that the proportionality constant does not change sign with variation in

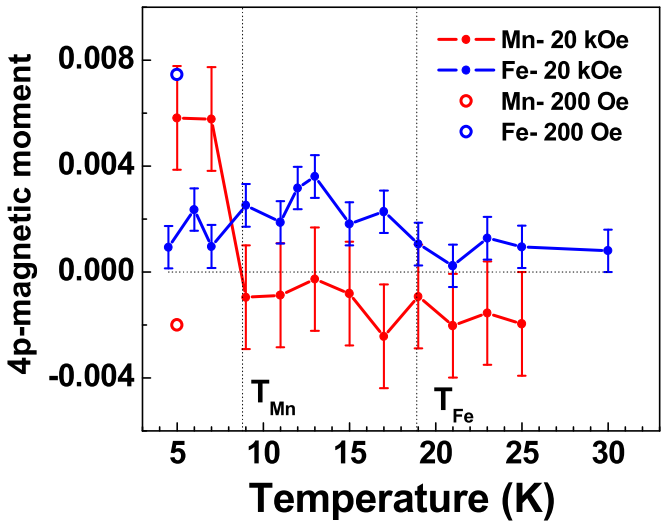

Figure 2. Temperature-dependence of (Fe, Mn) sub-lattice ordering at $H = 20$ kOe. Sublattice ordering temperatures $(T_{Mn},\ T_{Fe}) = (8.8\ K,\ 18.9\ K)$ are marked. The values of moment for $H = 200$ Oe and $T = 5.5$ K are also shown.

field and temperature. Thus, the controversies and complications of *K*-edge XMCD analysis do not alter our main results (presented in the following section), viz. different ordering temperatures for (Fe, Mn) sublattices and sign reversal for Mn moment.

XMCD-derived magnetic moments $\mu\,(H)$ carry spin cant angle (θ_{cant}) information. We show later that spin configuration is not exactly parallel (or anti-parallel) but *canted* in this system; spin canting results from a competition among several interaction forces [30, 31]. We calculate $(\theta_{cant})_{Fe,Mn}$ from the respective moment values at $T = 5.5$ K. For each sublattice, 0° (i.e. along field direction) is assigned to the maximum moment (μ^{max}) condition i.e. parallel alignment configuration. From Fe *K*-edge XMCD, $\mu^{max}_{Fe} = 0.0075$ at $H = 200$ Oe; we assign Fe-spin direction at $H = 200$ Oe as the reference field direction, and deduce: $\theta^{Fe}_{cant}(H) = \cos^{-1}(f_{Fe})$; $f_{Fe} = \mu_{Fe}(H)/\mu^{max}_{Fe}$. From Mn *K*-edge XMCD, $\mu^{max}_{Mn} = 0.006$ at $H = 20$ kOe, and $\theta^{Mn}_{cant}(H) = \cos^{-1}(f_{Mn})$; $f_{Mn} = \mu_{Mn}(H)/\mu^{max}_{Mn}$.

3. XMCD results

3.1. Temperature-dependence of sublattice magnetization

From the integrated areas of the XMCD peaks for the Mn and Fe edges at temperatures between 5 and 30 K and under $H = 20$ kOe, the derived temperature-dependent magnetic moments are plotted in figure 2. We find that (Fe, Mn) sublattices order sequentially in the following manner:

$$\begin{pmatrix}\text{Fe}+\text{Cu}\\ \text{Mn}\end{pmatrix}^{\text{ordered}}_{\text{ordered}} \xleftarrow[T_{Mn}\,=\,8.8\ \text{K}]{} \left\{\begin{pmatrix}\text{Fe}+\text{Cu}\\ \text{Mn}\end{pmatrix}^{\text{ordered}}_{\text{disordered}}\right\} \xleftarrow[T_{Fe}\,=\,18.9\ \text{K}]{} \begin{pmatrix}\text{Fe}+\text{Cu}\\ \text{Mn}\end{pmatrix}^{\text{disordered}}_{\text{disordered}}$$

i.e. Fe + Cu sublattice system is ordered below 18.9 K while Mn sublattice orders below 8.8 K. (The other details of figure 2 are discussed in supplementary material and figure S3.) In the present compound, magnetic ordering of sublattices at different temperatures directly defies the MFT theory; instead, the Mn sublattice appears to follow the Belov's 'weak' sublattice scheme [32]. Mn and Fe sublattice magnetic ordering temperatures, $(T_{Mn},\ T_{Fe}) \approx (T_{CR1},\ T_{CR2})$ strongly suggest that the observed multiple magnetic transitions in temperature dependent magnetization study shown in figure S1 [15–17], are directly correlated with sequential (Fe, Mn) sublattice magnetic ordering.

3.2. Magnetic field-dependence of sublattice magnetization at $T = 5.5$ K

3.2.1. Spin reversal across low → high field.

From figure 2, we note that in the ground state-($H = 200$ Oe), $(\mu_{Mn},\ \mu_{Fe}) = (-,\ +)$ i.e. the sign of Mn moment is negative; Mn and Fe moments are aligned in opposite directions, consistent with Fe–Mn antiferromagnetic (AFM) exchange coupling. In the flip state ($H = 20$ kOe), $(\mu_{Mn},\ \mu_{Fe})_{H=20\ kOe} = (+,\ +)$ i.e. Mn moment changes its sign to positive in figure 2. (Change in XMCD sign is clear from figure 1(b).) As a result of field induced sign reversal of Mn sublattice moment, the net magnetization changes from negative to positive, revealing a microscopic understanding of the observed field dependence of the macroscopic magnetization

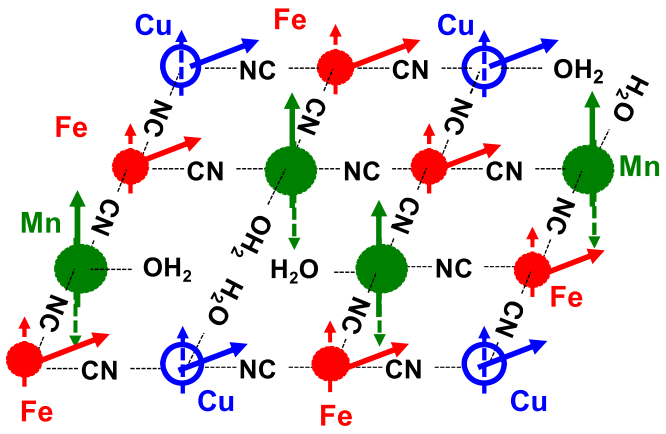

Figure 3. Spin configuration at $T = 5.5$ K, deduced from XMCD ($H = 20$ kOe) data analysis , is depicted by solid arrows. The dashed arrows represent the spin configuration at zero field as deduced from our low temperature (1.7 K) neutron diffraction study.

results (figure S1) [15–17]. It also confirms our original proposition that field actuated magnetization crossover (flip-flop) in the system arises from Mn spin flip. Ease of Mn spin flip could be correlated with its Mn^{2+} ($d^5 = t_{2g}^3 e_g^2$, $S = 5/2$) electronic state having no MAE due to zero orbital moment; MAE constants $K_{Mn} < K_{Fe}$. Besides, ZE (corresponding to 20 kOe applied magnetic field) is able to overcome the AFM E_{exch} between Fe and Mn moments. We clarify that Mn K-edge XANES remains unchanged between the two field (200 Oe and 20 kOe) conditions so that the role of charge reordering or change in valence state on magnetization reversal may be ruled out.

3.2.2. Spin cant angle at ($H = 20$ kOe, $T = 5.5$ K)

As defined in experimental details section, the spin cant angles are derived as follows:

$$\begin{matrix} |\mu_{Mn}|_{T=5.5\,K} = 0.006 \\ |\mu_{Fe}|_{T=5..5\,K} = 0.0025 \end{matrix} \Rightarrow \begin{matrix} f_{Mn} = 1 \\ f_{Fe} = 0.36 \end{matrix} \Rightarrow \begin{matrix} \theta_{Mn} = 0^\circ \\ \theta_{Fe} = 69^\circ \end{matrix}.$$

Spin configuration at $T = 5.5$ K, for both the zero field and 20 kOe field conditions, is depicted in figure 3. The mechanism of spin rotation can be explained in the following way: at high (20 kOe) field, the corresponding ZE ($ZE_{Mn} = \mu_{Mn} H \cos\theta = 0.41$ meV) assumes importance for the Mn sub-lattice below T_{Mn}. Stronger Mn moment ($S = 5/2$) compared to Fe moment ($S = 1.2$) now ensures a parallel (*with respect to* field) spin-alignment for Mn, while Fe–Mn AFM exchange coupling [15] compels Fe spin to rotate away from the field axis. The Fe moment direction under field is dictated by the competing ZE, E_{exch}, and MAE.

For $T > T_{Mn}$ in figure 2, $\mu_{Fe}(H = 20$ kOe$) \approx 0.003$ is significantly reduced from $\mu_{Fe}(H = 200$ Oe$) \approx 0.006$, resembling Fe spin canting ($\theta_{Fe} = 65^o$). Below $T_{Mn} = 8.8$ K i.e. with the onset of Mn sublattice ordering, Fe spin is further rotated away from 65° to 69° as the effective AFM exchange coupling (E_{exch}) strengthens. In principle, Fe spin canting should be absent in this temperature range ($T > T_{Mn}$) since Mn sublattice is supposedly disordered and therefore, Fe–Mn AFM exchange coupling is absent. In the absence of competing force, Fe spin should have aligned along field direction and $\mu_{Fe}(H = 20$ kOe$)$ should have assumed the maximum value for $T > T_{Mn}$. This leads us to the question whether the 'negative' values of Mn moment for $T > T_{Mn}$ (figure 2) are real or artifact. In principle, Mn moment values should have been 0 for a disordered sublattice. The fact that the negative Mn moment at $T > T_{Mn}$ is so close to 0 within error bar (figure 2) is well consistent with local canted (large cant angle) Mn spin configuration. Canted Mn spin would provide Fe–Mn AFM force to cant Fe spin and that would explain the observed reduced $\mu_{Fe}(H = 20$ kOe$)$. We add that bulk ordering of Mn moment is evident only at $T_{Mn} \leqslant 8.8$ K. As explained in details in supplementary material, the question (disordered versus local spin canted Mn sublattice) is not resolvable unambiguously due to large fluctuations in data. In our system, it is even possible that the observed Fe K-edge XMCD has contribution from Mn/Cu atoms at high field. If Mn sublattice is indeed completely disordered, one may have to explore the possibility of a K-edge XMCD artifact to explain the observed small $\mu_{Fe}(H = 20$ kOe$)$ [33, 34]. For the present work, it must be clarified that these discrepancies do not alter our main results, viz. different ordering temperatures for (Fe, Mn) sublattices and field-dependent sign reversal for Mn moment.

4. Discussions

Deviation from the MFT in terms of decoupling of (Fe, Mn) sublattices is evident as we have found different ordering temperatures for these sublattices, (T_{Mn}, T_{Fe}) $\approx$ (8.8 K, 18.9 K). Besides, we have found a spin reversal ($\theta = 180°$) of Mn sublattice alone at high field, whereas Fe-moment is found to cant only by 69° retaining its positive sign with respect to the applied magnetic field. Sublattice decoupling has been observed for the RE (4f)-TM (3d/5d) systems, $Ho_{0.5}Lu_{0.5}Fe_2$, $Er_{0.5}Y_{0.5}Fe_2$, $Gd_3Fe_5O_{12}$ and $Nd_{1-x}Ca_xMnO_3$ [7, 32, 35], understandably due to their varying characters viz. localized as well as anisotropic 4f versus delocalized 3d/5d orbitals. For the present case, though a simultaneous ordering of sublattices is reported for the 'two-sublattice' end compounds [$Mn_{1.5}Fe(CN)_6$/$Cu_{1.5}Fe(CN)_6$] of the present PBA series [16], a deviation from the MFT occurs for the present mixed composition viz. $Cu_{0.73}Mn_{0.77}Fe(CN)_6$. In order to understand this, we consider the large disparity in Fe coupling with Cu vis-à-vis Mn sublattice, viz. $J_{FeCu} \gg J_{FeMn}$ [16]. Under domination of this strong FM coupling, [Fe + Cu] can be perceived as a unified 'strong' sublattice. A much weaker (Fe–Mn) AFM coupling (J_{FeMn}) results in effective decoupling between Fe and Mn, and subsequently, in the separation of 'strong' [Fe + Cu] and 'weak' Mn sublattices, consistent with the Belov's model [32]. Due to this decoupling, Fe sublattice ordering temperature ($T_{Fe} = 18.9$ K) in $Cu_{0.73}Mn_{0.77}Fe(CN)_6$ is almost the same as that (=22 K) of the Fe–Cu end compound $Cu_{1.5}Fe(CN)_6$ and relatively insensitive to the presence of Mn neighbor. Further, one needs to investigate if the apparent sublattice decoupling could have resulted from inequivalent structural distortions around Fe and Mn atoms [34].

For the field dependent moment reversal phenomenon, additional energy terms viz. MAE ($K_{Mn} < K_{Fe}$), and magnetic moment ($\mu_{Mn} \gg \mu_{Fe}$) [15] need to be considered. Large ZE (ZI_{Mn}) at high field and lower K_{Mn} cumulatively reorient Mn moment from negative (as shown in figure 2) to positive. On the other hand, relatively strong K_{Fe} preserves positive sign for Fe moment. Consequently, the net magnetization changes sign: negative (−) [as ($\mu_{Mn} \gg \mu_{Fe}$)] $\rightarrow$ positive (+). Thus, magnetization reversal in this compound is a direct consequence of the sublattice decoupling i.e. deviation from the MFT.

5. Conclusion

Employing XMCD, we have investigated the microscopic origin of field-actuated magnetization reversal of PBA $Cu_{0.73}Mn_{0.77}Fe(CN)_6$. Our XMCD results reveal marked deviation of sublattice ordering from MFT in this system: (i) sequential, instead of common, ordering of (Fe, Mn) sublattices as function of temperature. This represents effective decoupling between the (Fe, Mn) sublattices. (ii) different responses of (Fe, Mn) sublattices to magnetic field, viz. moment reversal of Mn sublattice from negative to positive, while Fe moment retains its positive sign, and (iii) parallel versus canted (*with respect to* field direction) moment configuration for Mn and Fe sublattices, respectively. This decoupling is unusual, considering delocalized nature of 3d-orbitals; it occurs due to large disparity in sublattice coupling strengths, viz. 'strong' Fe − Cu versus 'weak' Fe–Mn coupling where inter-sublattice competition among different magnetic parameters (exchange coupling constant, MAE constant, and magnetic moment under field) plays an important role. The present system is indeed different from the earlier systems with localized f-orbital [7–12], and/or (multi-site) four sublattices [36–38]. We have conclusively drawn direct correlation between magnetization reversal (switching) and preferential Mn sublattice moment reorientation. Thus, magnetic switching in this system is a direct consequence of sublattice decoupling. Modeling of magnetization reversal mechanism necessitated non-exchange interaction terms, particularly the crucial role of magnetic anisotropy. The latter is remarkable for 3d-orbital cubic system. Finally, the methodology adopted in the present work is not limited to magnetization reversal alone but could be extended to spin reorientation, magnetic switching phenomena. Our results reveal that an optimization of the competing energy terms, Zeeman, exchange and magnetic anisotropy is necessary for design of future magnetic switches by exploiting the magnetization reversal phenomenon.

Acknowledgement

Work at Argonne was supported by the U.S. Department of Energy, Office of Science, under Contract No. DE-AC02-06CH11357.

References

[1] Kumar A and Yusuf S M 2015 The phenomenon of negative magnetization and its implications *Phys. Rep.* **556** 1
[2] Smart J S 1955 The Néel theory of ferrimagnetism *Am. J. Phys.* **23** 356–70
[3] Carvallo C *et al* 2010 Self reversal of magnetization in oceanic submarine basalts studied with XMCD *Geophys. Res. Lett.* **37** L11306

[4] Bartolomé F *et al* 2005 Element-specific magnetometry on negatively magnetized $NdMnO_{3+\delta}$ *J. Appl. Phys.* **97** 10A503
[5] Kulkarni P D *et al* 2011 Repeated magnetic compensation in single crystal of $Nd_{0.8}Gd_{0.2}Al_2$ and XMCD evidence for reversal in orientation of local moments at second transition *AIP Conf. Proc.* **1349** 1217
[6] Lahiri D *et al* 2013 XAFS understanding of 'repeated' magnetic compensation in $Nd_{0.8}Tb_{0.2}Al_2$ *J. Phys.: Conf. Ser.* **430** 012106
[7] Boada R, Piquer C, Laguna-Marco M A and Chaboy J 2010 Decoupling of the magnetic sublattices at the compensation point in R–Fe compounds *Phys. Rev.* B **82** 052407
[8] Chaboy J, Piquer C and Plugaru N 2007 Fe-57 Mossbauer and x-ray magnetic circular dichroism study of magnetic compensation of the rare-earth sublattice in $Nd_{2-x}Ho_xFe_{14}B$ compounds *Phys. Rev.* B **76** 134408
[9] Choi Y, Haskel D and Cady A 2006 Twisted magnetization states near the compensation temperature of Fe/Gd multilayers: anisotropy and surface-termination effects *Phys. Rev.* B **73** 174401
[10] Laguna-Marco M A, Chaboy J and Maruyama H 2005 Element-selective thermal x-ray magnetic circular dichroism study through the magnetic compensation temperature of Ho_6Fe_{23} *Phys. Rev.* B **72** 094408
[11] Chaboy J *et al* 2000 Fe *K*-edge x-ray magnetic circular dichroism study in R_6Fe_{23} (R = Ho and Y) compounds near compensation temperature *J. Appl. Phys.* **88** 336
[12] Dhesi S S, van der Laan G and Bencok P 2010 Spin- and orbital-moment compensation in the zero-moment ferromagnet $Sm_{0.974}Gd_{0.026}Al_2$ *Phys. Rev.* B **82** 180402
[13] http://google.com/patents/WO2013095139A2?cl=en
[14] Ohkoshi S-I *et al* 1999 Design and preparation of a novel magnet exhibiting two compensation temperatures based on molecular field theory *Phys. Rev. Lett.* **82** 1285
[15] Kumar A, Yusuf S M, Keller L and Yakhmi J V 2008 Microscopic understanding of negative magnetization in Cu, Mn, and Fe based prussian blue analogues *Phys. Rev. Lett.* **101** 207206
[16] Yusuf S M, Kumar A and Yakhmi J V 2009 Temperature- and magnetic-field-controlled magnetic pole reversal in a molecular magnetic compound *Appl. Phys. Lett.* **95** 182506
[17] Yusuf S M, Kumar A and Yakhmi J V 2010 Bipolar magnetization switching and its control in a Prussian blue type molecular magnetic compound *J. Phys.: Conf. Ser.* **200** 022073
[18] Hu J M, Li Z, Chen L Q and Nan C W 2011 High-density magnetoresistive random access memory operating at ultralow voltage at room temperature *Nat. Commun.* **2** 553
[19] Yu B, Liu M, Egolf P W and Kitanovski A 2010 A review of magnetic refrigerator and heat pump prototypes built before the year 2010 *Int. J. Refrig.* **33** 1029
[20] Heer C V, Barnes C B and Daunt J G 1953 Magnetic refrigerator for maintaining temperatures below 1 K *Phys. Rev.* **91** 412
[21] Tušek J, Zupan S, Prebil I and Poredoš A 2009 Magnetic cooling—development of magnetic refrigerator *J. Mech. Eng.* **55** 5
[22] Schu¨tz G *et al* 1987 Absorption of circularly polarized x-rays in iron *Phys. Rev. Lett.* **58** 737
[23] Ohkoshi S I, Arai K, Sato Y and Hashimoto K 2004 Humidity-induced magnetization and magnetic pole inversion in a cyano-bridged metal assembly *Nat. Mater. Lett.* **3** 857
[24] Igarachi K J I and Hirai K 1994 Magnetic circular dichroism at the *K* edge of nickel and iron *Phys. Rev.* B **50** 17820
[25] Guo G Y 1996 What does the *K*-edge x-ray magnetic circular dichroism spectrum tell us? *J. Phys.: Condens. Matter* **8** L747
[26] Chaboy J *et al* 1998 X-ray magnetic-circular-dichroism probe of a noncollinear magnetic arrangement below the spin reorientation transition in $Nd_2Fe_{14}B$ *Phys. Rev.* B **57** 8424
[27] Sanders R E Jr 2001 Technology innovation in aluminium products *JOM* **53** 21–5
ASM Material Datasheet (http://asm.matweb.com/search/SpecificMaterial.asp?bassnum=MA6061t6)
[28] Freeland J W *et al* 2002 A unique polarized x-ray facility at the advanced photon source *Rev. Sci. Instrum.* **73** 1408
[29] Suzuki M *et al* 1998 Helicity-modulation technique using diffractive phase retarder for measurements of x-ray magnetic circular dichroism *Japan. J. Appl. Phys.* **37** L1488
[30] Garcia L M, Chaboy J, Bartolomé F and Goedkoop J B 2000 Orbital magnetic moment instability at the spin reorientation transition of $Nd_2Fe_{14}B$ *Phys. Rev. Lett.* **85** 429
[31] Grazioli C *et al* 2005 Spin-flop ordering from frustrated ferro- and antiferromagnetic interactions: a combined theoretical and experimental study of a Mn/Fe(100) monolayer *Phys. Rev. Lett.* **95** 117201
[32] Belov K P 1996 Ferrimagnets with a 'weak' magnetic sublattice *Phys.—Usp.* **39** 623
[33] Boada R, Piquer C, Laguna-Marco M A and Chaboy J 2010 Additivity of magnetic contributions to the x-ray magnetic circular dichroism spectrum *Phys. Rev.* B **81** 100404(R)
[34] Cafun J-D, Lejeune J, Itie J-P, Baudelet F and Bleuzen A 2013 XMCD at the transition metal *K*-edges as a probe of small pressure-induced structural distortions in prussian blue analogues *J. Phys. Chem.* C **117** 19645
[35] Troyanchuk I O *et al* 2003 Spin-reorientational transitions in low-doped $Nd_{1-x}Ca_xMnO_3$ manganites: the evidence of an inhomogeneous magnetic state *J. Phys.: Condens. Matter* **15** 8865
[36] Yunus S M, Shim H S, Lee C H, Asgar M A, Ahmed F U and Zakaria A K M 2001 Neutron diffraction studies of the diluted spinel ferrite $ZnxMg_{0.75}-xCu_{0.25}Fe_2O_4$ *J. Magn. Magn. Mater.* **232** 121
[37] Yunus S M, Shim H S, Lee C H, Asgar M A, Ahmed F U and Zakaria A K M 2002 Investigation of the magnetic structure of the spinel compound $Zn_xCu_{1-x}FeCrO_4$ by neutron diffraction *J. Magn. Magn. Mater.* **241** 40
[38] Zakaria A K M, Asgar M A, Eriksson S G, Ahmed F U, Yunus S M and Rundlöf H 2003 The study of magnetic ordering in the spinel system $Zn_xNi_{1-x}FeCrO_4$ by neutron diffraction *J. Magn. Magn. Mater.* **265** 311